Calculation of Differential Reflection Coefficient for Isolated Microscopic Well Structure

Jong Tai Lee[a)]

We have calculated differential reflection coefficient for isolated well structure of micro-scale, etched on dielectric surface. The differential reflection coefficient is computed using Green's second integral theorem. The purpose of our computation is to find a class of well profiles which give maximal diffusive scattering. To have such a maximal effect, we have concluded that the waist radius of Gaussian beam and its wavelength should be comparable to the well width and that well depth has to be larger than a wavelength. Exact calculation of differential reflection coefficients of dielectric surface with isolated structure on it may be used for the examination of dielectric surfaces and also in making simple but efficient diffuser.

I. INTRODUCTION

The enhanced backscattering from a large amplitude random grating was calculated by Maradudin *et al*. based on Green's second integral theorem [1]. Their formalism is so powerful to naturally take account of surface shadowing and multiple scattering. To resemble the experimental setup, they also used the incident Gaussian beam with waist radius comparable to the sample size, thereby eliminating periodic replication of the sample surface as is the case in the scattering of plane wave. The Maradudin's formalism draws a set of two integral equations which can be solved numerically. Their numerical solution confirmed the enhanced peak at back-scattering angle [2], which has been experimentally observed. One early formalism that has been used with some success is that of Beckmann and Spizzichino [3], which uses so-called Kirchhoff approximation. But the approximation fails completely if the surface correlation scale a is comparable with the wavelength $ë$. Further, this theory does not take account of multiple scattering or surface shadowing. The other several formalisms have been made up and compared with the experimental results, namely, the small perturbation method and extinction theorem method. But these formalisms have their own limitations. The enhanced backscattering from deterministic surfaces instead of random grating has also been observed [4], [5]. It is quite surprising to have enhanced back-scattering from deterministic surfaces. The main conclusion out of their efforts is that the enhanced backscattering is due to multiple scattering from deep grooves. The multiply scattered optical paths with their time reversed ones give us constructive interference at backscattering angle. So it will be interesting to compute differential reflection coefficient (DRC) from an isolated, large amplitude groove on dielectric surface and to see whether we can still have any sign of enhanced backscattering.

Manuscript received Septemper 1, 1998; revised August 27, 1999.

[a)]Electronic mail: jtl@etri.re.kr.

In this paper, an isolated well is introduced on the dielectric surface with varying its depth, width or wall slope. The resulting DRC's are obtained and analyzed to look for correlation with well shape. The lateral size of well is comparable to wavelength used so that we are in the diffractive regime. The simple geometric optics can not be applied to this system. Instead we used Maradudin's formlism to compute DRC by applying Gaussian beam on the sample surface. Our results show that we do not have any sign of enhanced back-scattering. But when the waist radius of incident beam is comparable to well width, DRC obviously deviates from specular reflection, becoming a good candidate for efficient diffuser. This model calculation can be applied to examine real sample surfaces also. We briefly describe theoretical back-grounds in Section II. In section III, the numerical results are shown and examined. Section IV concludes this paper.

II. THEORETICAL BACKGROUND

We consider the p-polarized electromagnetic field incident from the vacuum side onto the dielectric surface defined by $x_3 = \hat{\imath}(x_1)$ with the plane of incidence of x_1x_3-plane. The vacuum is at $\epsilon_3 > \hat{\imath}(x_1)$ and material $x_3 < \hat{\imath}(x_1)$. The material side has a dynamic dielectric function $\hat{a}(\omega)$. The magnetic and electric fields have the form

$$H(\tilde{n},t) = (0, H_2(\tilde{n}), 0)\exp(-i\omega t), \tag{1}$$

$$E(\tilde{n}, t) = (E_1(\tilde{n}),\ 0,\ E_3(\tilde{n}))\exp(-i\omega t). \tag{2}$$

Translational symmetry in x_2-direction is implied and $\tilde{n} = (x_1, x_3)$. Because time dependence is explicitly shown through exponential term, hereafter any derivative ∂_t in time will be replaced with $-i\omega$. $H_2(\tilde{n})$ is the solution of the equations

$$\left(\partial_1^2 + \partial_3^2 + \frac{\omega^2}{c^2}\right) H_2^{>}(\tilde{n}) = 0, \quad x_3 > \hat{\imath}(x_1), \tag{3}$$

$$\left(\partial_1^2 + \partial_3^2 + \hat{a}(\omega)\frac{\omega^2}{c^2}\right) H_2^{<}(\tilde{n}) = 0, \quad x_3 < \hat{\imath}(x_1), \tag{4}$$

where ∂_i is equivalent to $\partial/\partial x_i$. The boundary condition satisfied by $H_2^{>}(\tilde{n})$ and $H_2^{<}(\tilde{n})$ at the interface are

$$H_2^{>}(\tilde{n})\big|_{\hat{\imath}(x_1)} = H_2^{<}(\tilde{n})\big|_{\hat{\imath}(x_1)}, \tag{5}$$

$$\frac{\partial}{\partial n_+} H_2^{>}(\tilde{n})\big|_{\hat{\imath}(x_1)} = \frac{1}{\hat{a}(\omega)}\frac{\partial}{\partial n_+} H_2^{<}(\tilde{n})\big|_{\hat{\imath}(x_1)}, \tag{6}$$

where $\partial/\partial n_+$ is normal derivative at the surface, pointing from material to vacuum side. The $H_2^{>}(\tilde{n})$ at $x_3 \to +\infty$ consists of an incoming and outgoing waves, while $H_2^{<}(\tilde{n})$ at $x_3 \to -\infty$ is exponentially decaying wave.

We now introduce two Green functions, $G_o(\tilde{n},\tilde{n}')$ and $G_{\hat{a}}(\tilde{n},\tilde{n}')$ satifying

$$\left(\partial_1^2 + \partial_3^2 + \frac{\omega^2}{c^2}\right) G_o(\tilde{n},\tilde{n}') = -4\pi\delta(\tilde{n}-\tilde{n}'), \tag{7}$$

$$\left(\partial_1^2 + \partial_3^2 + \frac{\hat{a}(\omega)\omega^2}{c^2}\right) G_{\hat{a}}(\tilde{n},\tilde{n}') = -4\pi\delta(\tilde{n}-\tilde{n}'). \tag{8}$$

The $G_o(\tilde{n},\tilde{n}')$ and $G_{\hat{a}}(\tilde{n},\tilde{n}')$ have solutions of Hankel function of $i\pi H_o^{(1)}(r)$ and $i\pi H_o^{(1)}(\sqrt{\hat{a}}r)$ respectively, in which $r = (\omega/c)\sqrt{(x_1-x_1')^2 + (x_3-x_3')^2}$. By applying Green's second integral theorem to vacuum side, we can have inhomogeneous integral equation of

$$\begin{aligned}\epsilon\,(x_3 - \hat{\imath}(x_1))H_2^{>}(\tilde{n}) &= H_2^{>}(\tilde{n})_{inc} \\ &+ \frac{1}{4\pi}\int_{-\infty}^{\infty} dx_1'\Big[H_2^{>}(\tilde{n}')(-\hat{\imath}'(x_1')\partial_1' + \partial_3')G_o(\tilde{n},\tilde{n}') \\ &- G_o(\mathbf{r},\mathbf{r}')(-\hat{\imath}'(x_1')\partial_1' + \partial_3')H_2^{>}(\tilde{n}')\Big]_{x_3'=\hat{\imath}(x_1')}.\end{aligned} \tag{9}$$

The integral term of r.h.s. represents scattered field, $H_{2,sc}$. The similar procedure is applied to material field $H_2^{<}(\tilde{n})$ so that we have

$$\begin{aligned}\epsilon(\hat{\imath}(x_1) - x_3)H_2^{<}(\tilde{n}) &= \\ &-\frac{1}{4\pi}\int_{-\infty}^{\infty} dx_1'\Big[H_2^{>}(\tilde{n}')(-\hat{\imath}'(x_1')\partial_1' + \partial_3')G_{\hat{a}}(\tilde{n},\tilde{n}') \\ &-\hat{a}(\omega)G_{\hat{a}}(\tilde{n},\tilde{n}')(-\hat{\imath}'(x_1')\partial_1' + \partial_3')H_2^{>}(\tilde{n}')\Big]_{x_3'=\hat{\imath}(x_1')}.\end{aligned} \tag{10}$$

By defining two source terms

$$H(x_1) = H_2^{>}(\mathbf{r})\big|_{x_3=\xi(x1)}, \tag{11}$$

$$L(x_1) = (-\hat{\imath}'(x_1)\partial_1 + \partial_3)H_2^{>}(\tilde{n})\big|_{x_3=\hat{\imath}(x_1)}, \tag{12}$$

and

$$H_o(x_1,x_1') = \lim_{\hat{a}\to 0_+}\frac{1}{4\pi}(-\hat{\imath}'(x_1')\partial_1' + \partial_3')G_o(\tilde{n},\tilde{n}')\big|_{x_3=\hat{\imath}(x_1)+\hat{a},\, x_3'=\hat{\imath}(x_1')}, \tag{13}$$

$$L_o(x_1,x_1') = \lim_{\ddot{a}\to 0_+}\frac{1}{4\eth} G_o(\tilde{n},\tilde{n}')\Big|_{x_3=\hat{\imath}(x_1)+\ddot{a},\ x_3'=\hat{\imath}(x_1')}, \quad (14)$$

$$H_{\mathring{a}}(x_1,x_1') = \lim_{\ddot{a}\to 0_+}\frac{1}{4\eth}(-\hat{\imath}'(x_1')\partial_1' + \partial_3')G_{\mathring{a}}(\tilde{n},\tilde{n}')\Big|_{x_3=\hat{\imath}(x_1)+\ddot{a},\ x_3'=\hat{\imath}(x_1')}, \quad (15)$$

$$L_{\mathring{a}}(x_1,x_1') = \lim_{\ddot{a}\to 0_+}\frac{1}{4\eth} G_{\mathring{a}}(\tilde{n},\tilde{n}')\Big|_{x_3=\hat{\imath}(x_1)+\ddot{a},\ x_3'=\hat{\imath}(x_1')}, \quad (16)$$

we can transform (9) and (10) into

$$H(x_1) = H(x_1)_{inc} + \int_{-\infty}^{\infty} dx_1'\left[H_o(x_1,x_1')H(x_1') - L_o(x_1,x_1')L(x_1')\right], \quad (17)$$

$$0 = \int_{-\infty}^{\infty} dx_1'\left[H_{\mathring{a}}(x_1,x_1')H(x_1') - \mathring{a}(\grave{u})L_{\mathring{a}}(x_1,x_1')L(x_1')\right]. \quad (18)$$

This is a set of integral equations to be solved to compute DRC. H_o and L_o are obtained by setting $\mathring{a}=1$. We put the observation point just above the surface, which was represented by introducing positive infinitesimal, $\ddot{a}$.

Now we have the total, time-averaged, scattered flux of

$$P_{sc} = \int dx_1 \int dx_2\, \mathrm{Re}\left[-i\frac{c^2}{8\eth\mathring{\mathrm{a}}\grave{u}} H_{2,sc}^{*}(\partial_3 H_{2,sc})\right]_{x_3>\max(\hat{\imath}(x_1))}. \quad (19)$$

By definition, DRC is given by

$$\frac{1}{|P_{inc}|}\frac{\partial P_{sc}}{\partial \grave{e}_s} = \frac{c}{8\eth\grave{u}\,(8\eth|P_{inc}|/cL_2)}\left|r_p(k)\right|^2, \quad (20)$$

where

$$r_p(k) = \int_{-\infty}^{\infty} dx_1' e^{-ikx_1' - ia_0(k)\xi(x_1')} \times\left\{ i[k\hat{\imath}'(x_1') - a_o(k)]H(x_1') - L(x_1')\right\}, \quad (21)$$

and

$$\alpha_o(k) = \left(\frac{\grave{u}^2}{c^2} - k^2\right)^{1/2}, \quad k^2 < \frac{\grave{u}^2}{c^2}, \quad (22)$$

$$= i\left(k^2 - \frac{\grave{u}^2}{c^2}\right)^{1/2}, \quad k^2 > \frac{\grave{u}^2}{c^2}. \quad (23)$$

In (20), $|P_{inc}|$ is total, time-averaged power of an incident beam. The total DRC may be obtained by integrating (20) over all scattering angles in the vacuum side. The sample dismension was assumed to be $L_1 \times L_2$.

To compute DRC, we have to solve for $H(x_1)$ and $L(x_1)$ from (17) and (18). The coupled integral equations can be solved numerically by transforming integral equations to matrix forms [1], [6].

$$\mathbf{H} = \mathbf{H}_{inc} + \mathbf{H}^{(0)}\mathbf{H} - \mathbf{L}^{(0)}\mathbf{L}, \quad (24)$$

$$0 = \mathbf{H}^{(\mathring{a})}\mathbf{H} - \mathring{a}\mathbf{L}^{(\mathring{a})}\mathbf{L}, \quad (25)$$

where $\mathbf{H}$, $\mathbf{L}$ and $\mathbf{H}_{inc}$ are column vectors. When computing diagonal elements, singularity should be treated carefully [1]. The above coupled matrix equations have formal solutions of in the following way.

$$\mathbf{H} = \left[\mathbf{I} - \mathbf{H}^{(0)} + \frac{1}{\mathring{a}}\mathbf{L}^{(0)}\mathbf{L}^{(\mathring{a})-1}\mathbf{H}^{(\mathring{a})}\right]^{-1}\mathbf{H}_{inc}, \quad (26)$$

$$\mathbf{L} = \frac{1}{\mathring{a}}\mathbf{L}^{(\mathring{a})-1}\mathbf{H}^{(\mathring{a})}\mathbf{H}. \quad (27)$$

The 2-dimensional Gaussian wave $H_{2,inc}(x,z)$ is obtained from paraxial Helmholz equation [7] of

$$\left(\partial_x^2 - 2i\frac{\grave{u}}{c}\partial_z\right)H_{2,inc}(x,z) = 0. \quad (28)$$

With a depth of focus of z_o called Rayleigh range in 2-dim version $H_{2,inc}(x,z)$ has a general solution of

$$H_{2,inc}(x,z) = \sqrt{\frac{W_o}{W}}\exp\left[-\frac{x^2}{W^2}\right]\exp\left[-i\frac{\grave{u}}{c}\left(z + \frac{x^2}{2R}\right) + \frac{i}{2}\tan^{-1}\left(\frac{z}{z_o}\right)\right], \quad (29)$$

in which $R(z) = z\left[1 + (z_o/z)^2\right]$ is called radius of curvature of wavefront, $W(z) = W_o\left[1 + (z/z_o)^2\right]^{1/2}$ beam radius and $W_o = (\ddot{e}z_o/\eth)^{1/2}$ waist radius. If an incident beam is illuminated with incidence angle $\grave{e}_i$, which is measured from z axis in counterclockwise direction, x and z will be replaced by the relation of

$$\begin{pmatrix} x \\ z \end{pmatrix} = \begin{pmatrix} \cos\theta_i & \sin\theta_i \\ -\sin\theta_i & \cos\theta_i \end{pmatrix}\begin{pmatrix} x_1 \\ x_3 \end{pmatrix}, \quad (30)$$

At $x_3 = 0$ plane, we compute $|P_{inc}|$. From 29 and 30, we should get

$$|P_{inc}| = L_2\frac{c}{8\eth}\int dx_1 \frac{W_o}{W}e^{-2x^2/W^2}\frac{\partial}{\partial x_3}\left[z + \frac{x^2}{2R} - \frac{c}{2\grave{u}}\tan^{-1}\left(\frac{z}{z_o}\right)\right]_{x_3=0} \quad (31)$$

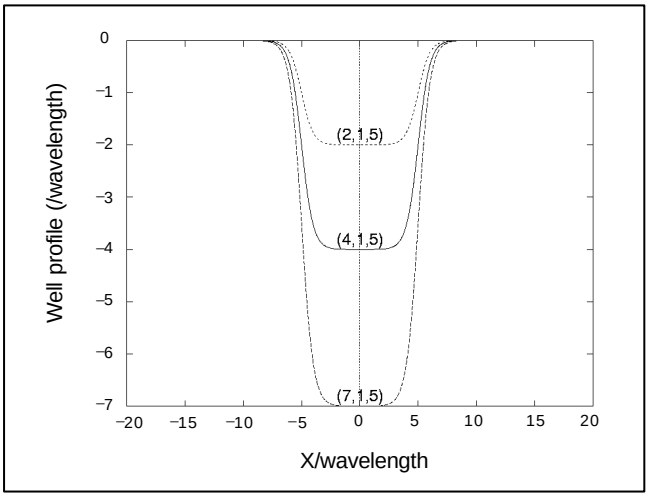

Fig. 1. The surface profiles of (A, 1, 5) are shown.

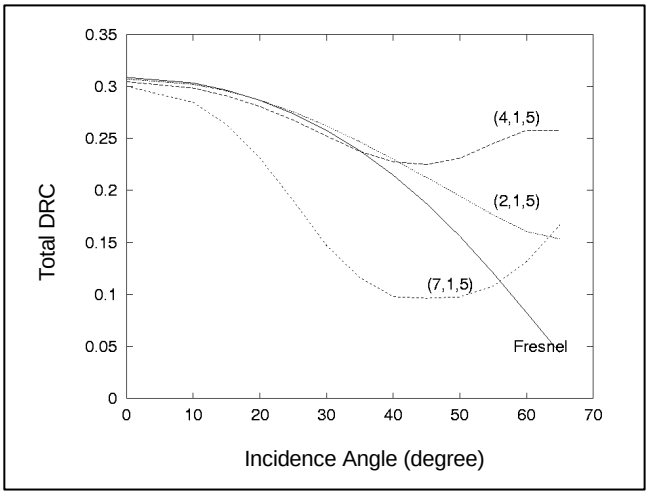

Fig. 2. For (A, 1, 5) case, Total DRC's are shown. Fresnel result is also shown for comparison.

in which partial derivative with respect to x_3 will become

$$\partial_3[\cdots]_{x_3=0} = \cos\theta_i \left[1 - \frac{x^2(z^2 - z_o^2)}{2(z^2 + z_o^2)^2} - \frac{c}{2\omega} \frac{z_o}{z^2 + z_o^2}\right] + \sin\theta_i \left[\frac{xz}{z^2 + z_o^2}\right], \quad (32)$$

where $x = \cos\theta_i x_1$ and $z = -\sin\theta_i x_1$. If z_o goes to infinity, we surely retrieve the result of plane wave, $L_1 L_2 c \cos\theta_i / 8\pi$. $|P_{inc}|$ will be obtained numerically.

III. RESULTS AND DISCUSSIONS

In this section, we compute DRC of a single 1-dimensional well etched on flat surface. The well is represented by differentiable scalar function. We have chosen a product of two hyperbolic tangents as the well,

$$\hat{\imath}(x_1) = A\left[\tanh B(x_1 + C) + 1\right]\left[\tanh B(x_1 - C) - 1\right], \quad (33)$$

where A, B and C are all positive numbers. A is for well depth, B wall slope and C well width. By varying A, B and C in arbitrary way, we can have smooth and differentiable wells of various shapes. So we will represent a particular well profile using a triad of (A, B, C) hereafter. The incident Gaussian beam illuminated on the groove is p-polarized, whose wavelength is 0.62 μm. The waist radius of the beam is set to be 1.86 μm, The corresponding Rayleigh range is about 28 μ. The bulk material has dielectric constant of 12.25 (typical value of Si), for which imaginary part is neglected.

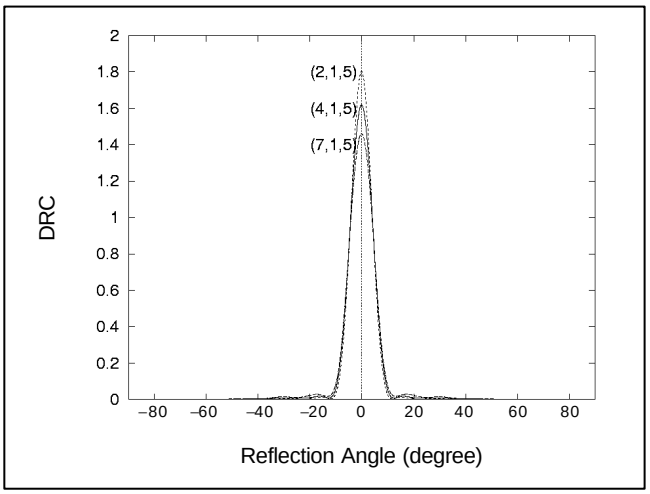

Fig. 3. For (A, 1, 5), incidence angle is fixed to 0°.

From many possible combinations of (A, B, C), we choose a reference profile of $A = 4\mu$, $B = \mu$ and $C = 5\mu$. We also fix the sample width to be 70 μ and divide the whole sample width into 2000 steps. These values are based on the parameters of the Gaussian beam as defined above. Because we want the beam center to be always located at coordinate origin and to be completely enclosed by well mouth, the waist radius has to be less than or comparable to the well width. The covering area by the incident field on sample surface increases as the incident angle increases. So the sample width must be large enough to accept all the incident fields. We found that 70 μ was reasonable width to get convergent result in computing DRC even up to 65°. Furthermore 2000 steps were large enough to take account of the spatial variations of fields and well profile. To check the computer program works fine, we first applied it to the flat surface, then computed DRC's from 0° up to 65°. For the flat surface, we have exact

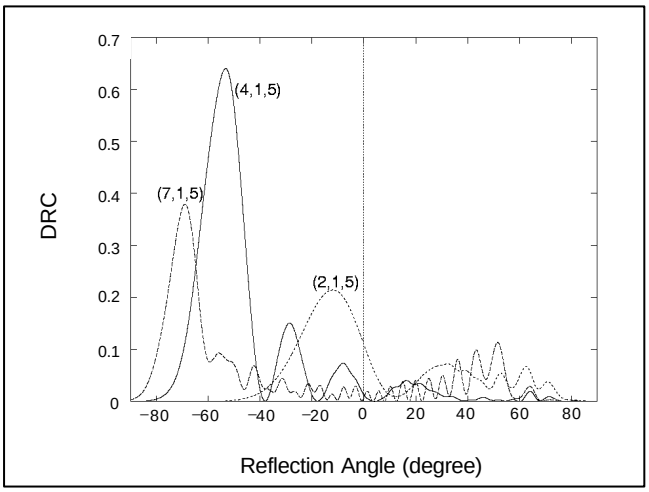

Fig. 4. For (A, 1, 5) case, incidence angle is fixed to 65°.

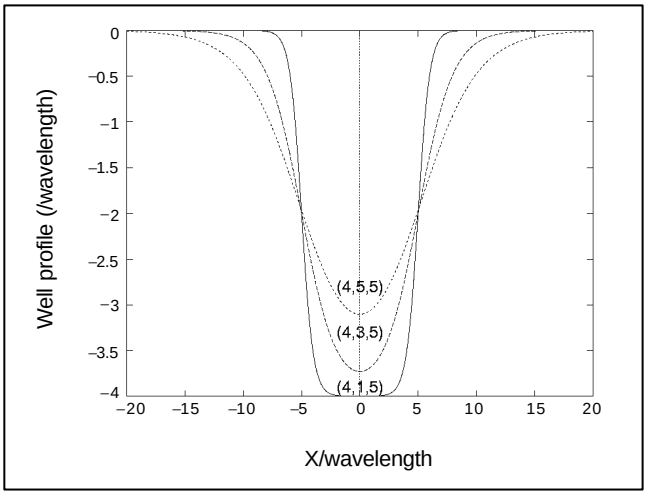

Fig. 6. The surface profiles of (4, B, 5) are shown.

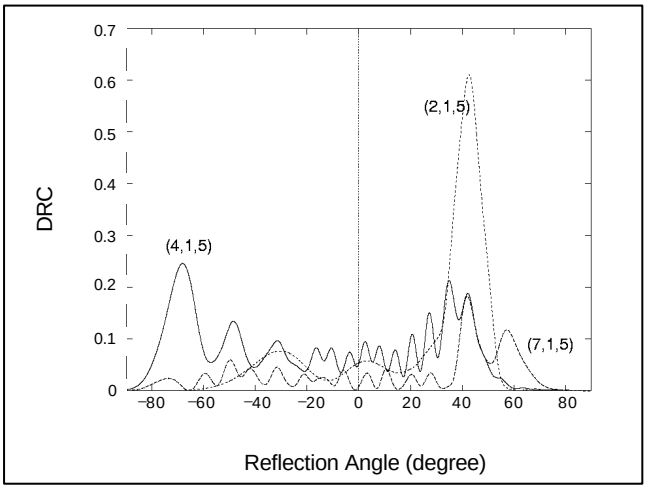

Fig. 5. For (A, 1, 5) case, incidence angle is fixed to 45°.

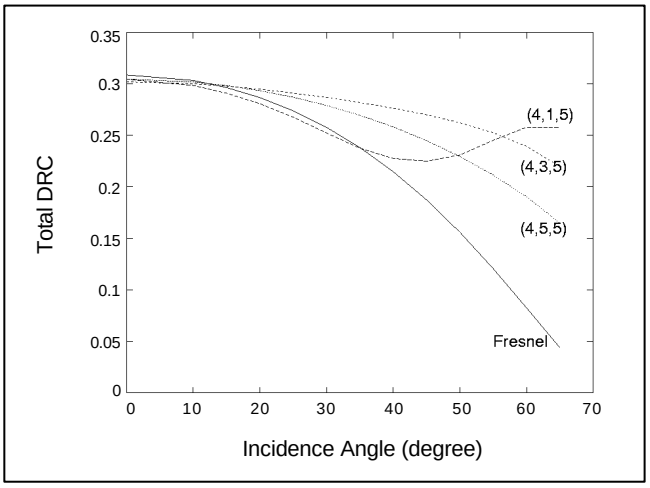

Fig. 7. Only B is changed. Fresnel result is also shown for comparison.

expression for reflection coefficient,

$$R = \left| \frac{n^2 \cos\grave{e}_i - \sqrt{n^2 - \sin^2 \grave{e}_i}}{n^2 \cos\grave{e}_i + \sqrt{n^2 - \sin^2 \grave{e}_i}} \right|^2 . \qquad (34)$$

The actual computation shows that the total DRC at each $\grave{e}_i$ does differ from Fresnel result within less than 1 %.

Fist of all we compute DRC by varying A only. Three different values of A are chosen. Surface profiles are shown in Fig. 1. B and C are fixed to $\ddot{e}$ and $5\ddot{e}$ respectively. The total reflection coefficient into the vacuum side at various reflection angles up to 65° are shown in Fig. 2. Fresnel reflection coefficient of (34) is also shown in the same plot for comparison. At small $\grave{e}_i$'s, the reflection coefficient is close to Fresnel result, but gradually deviating as $\grave{e}_i$ increases. We now look at DRC at normal incidence in Fig. 3. No particular structures are seen except strong specular reflection. It seems that the incident beam is not much affected by the well. But it is understandable if we compare the beam waist radius with well width. The beam waist radius is much smaller than the width of well bottom. That's why DRC's are more or less Fresnel-like.

Figure 2 shows two distinct features at large incidence angles. One is that, around 45°, (4, 1, 5) and (7, 1, 5) have local minima. The other one is that total DRC does not vanish even at Brewster's angle, which is about 74°, but increases. The latter one is due to the fact that well's wall is illuminated at different angle rather than Brewster's angle. It becomes evident from Fig. 4. The specular reflection is barely seen. Instead we see enhanced peak in the backscattering direction. These peaks can be understood with geometrical optics. Because the beam waist radius is small enough to illuminate particular position on wall, the incident energy is specularly reflected. That's why we

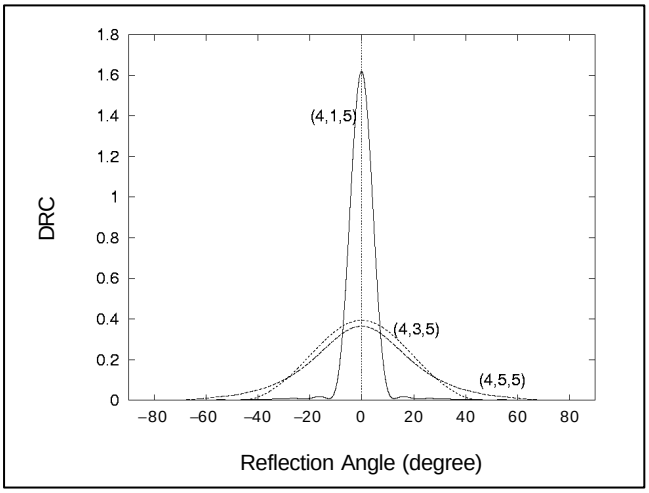

Fig. 8. Only B is changed. The incidence angle is fixed at 0°.

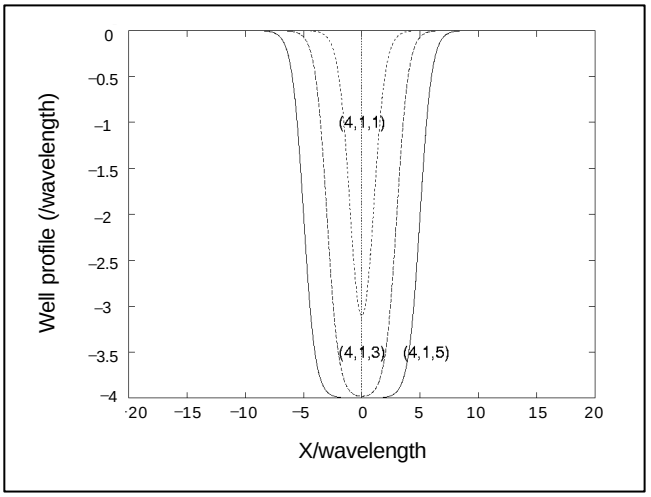

Fig. 10. The surface profiles of (4, 1, C) are shown.

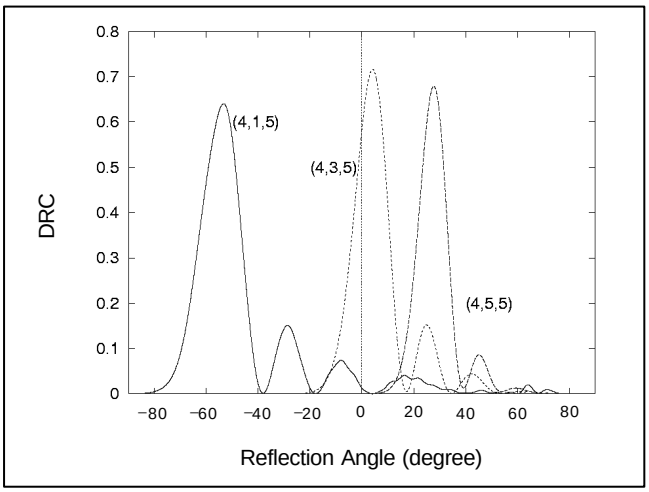

Fig. 9. Only B is changed. The incidence angle is fixed at 65°.

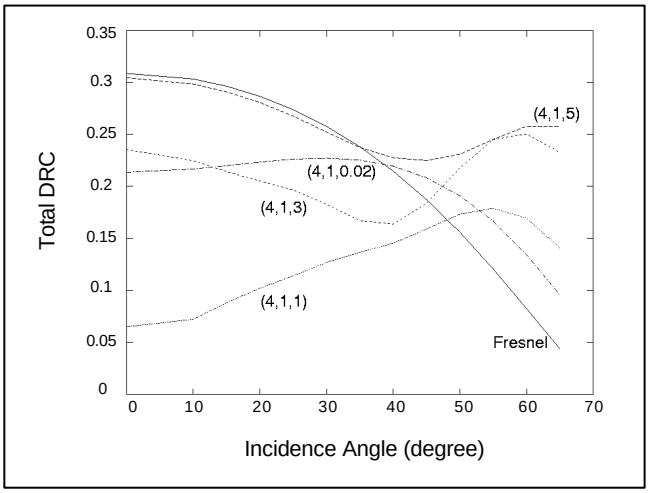

Fig. 11. Only C is changed. Fresnel result is also shown for comparison.

have prominent peaks in Fig. 4. Understanding the former one is also based on the same reasoning. Qualitatively saying, as we increase $\grave{e}_i$ from 0°, the actual incidence angle on wall decreases from 90°. So before we get to $\grave{e}_i$ = 74°, we should be able to see a minimum. But because the incident beam has a finite waist radius and wall's slope depends on position, we can not say that the minimum will show up at $\grave{e}_i$ = 16°. Only actual computation tells us local minimum angle.

Figure 5 plots DRC' s when $\grave{e}_i$ = 45°. We now have specular peak at $\grave{e}_r$ = 45° for (2, 1, 5), revealing the tendency of convergence to the case of flat surface. Other profiles let incident energy be scattered off into various angles. It should be understood as a result of multiple scattering. The fields trapped in the well is multiply reflected back and forth then finally some portion of the field energy escapes into the vacuum. The multiply reflected fields are coherently interferes with itself, thereby producing highly complicated structure of DRC.

Now let' s examine (4, B, 5) cases. With $A = 4\,\ddot{e}$ and $C = 5\,\ddot{e}$ fixed, only wall slope varies. Figure 6 shows three different surface profiles. We plot total DRC' s for them in Fig. 7. Except (4, 1, 5), we do not see any interesting features here. At small incidence angles total reflection coefficient is not much different from Fresnel result. But because the well bottom is not flat now, Fresnel peak is broadened as shown in Fig. 8. The smoothness of DRC means that almost no multiple scattering effects take place here. The structures of DRC' s in Fig. 9. are much simpler compared to Fig. 4. As mentioned above, because waist radius is small enough to be specularly reflected from a certain position of wall, we have specular peaks at different reflection angles even for the same incidence angle. Of course, as we increase the wall slope, we should recover the Fresnel result.

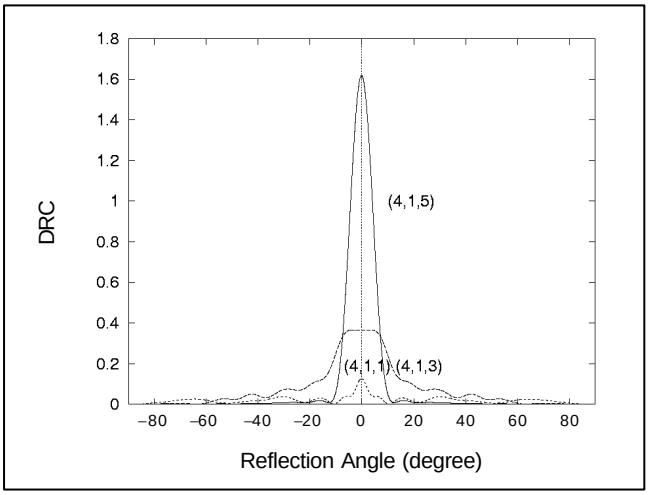

Fig. 12. For (4, 1, *C*) case, DRC's are shown when $\grave{e}_i = 0^\circ$.

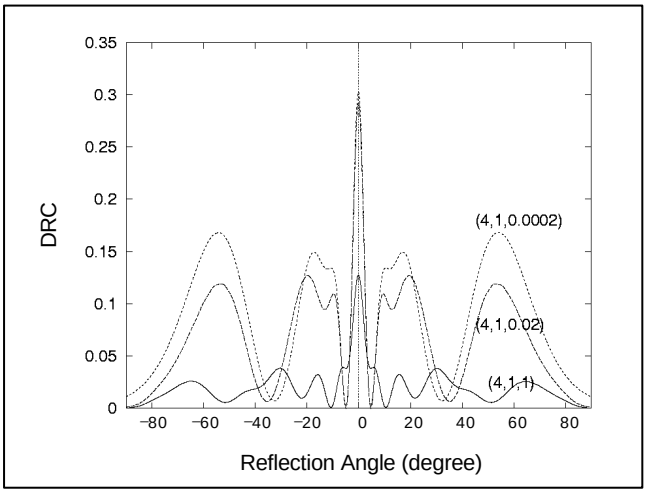

Fig. 13. For (4, 1, *C*) case, DRC's are shown when $\grave{e}_i = 0^\circ$.

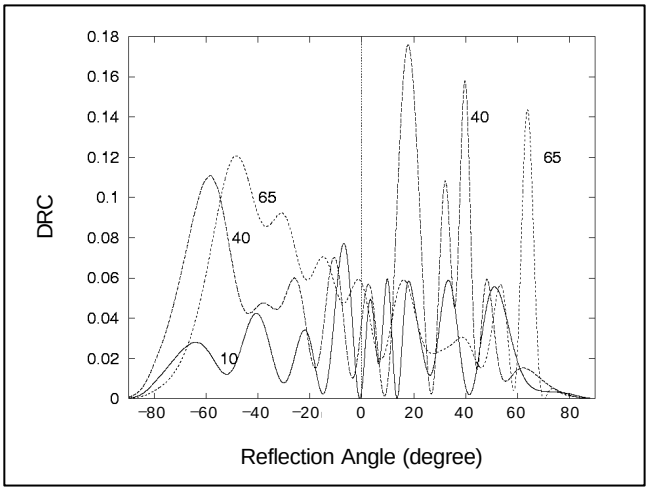

Fig. 14. For (4, 1, 1) profile, DRC's are shown when $\grave{e}_i = 10^\circ$, 40° and 65°.

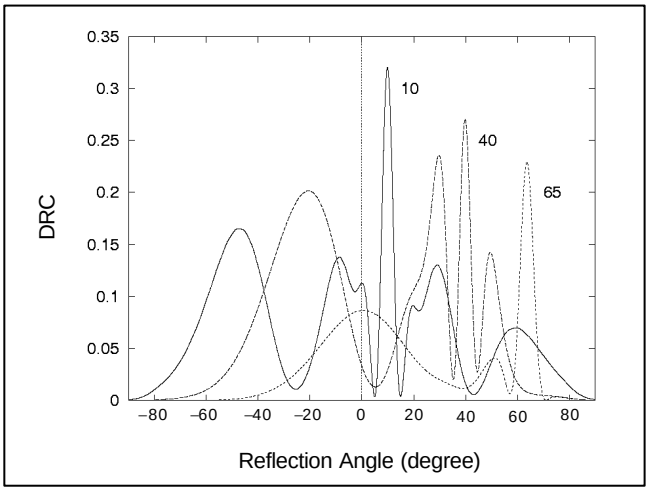

Fig. 15. For (4, 1, 0.02) profile, DRC's are shown when $\grave{e}_i = 10^\circ$, 40° and 65°.

Now consider well width dependence of DRC. We fix $A = 4\,\ddot{e}$ and $A = \ddot{e}$ but vary C only. Figure 10 compares three surface profiles and Fig. 11 total DRC's. At small incidence angles, we recognize that the dependence of DRC on well width is much different from those on its depth or slope. With gradual decrement of the well width, the total DRC at small angles decreases too, then turns upward converging to Fresnel result. Note that Fig. 11 has (4, 1, 0.02) case also. Before we understand this behavior, we first look at DRC's at normal incidence. Figure 12 shows that the strength of DRC of (4, 1, 1) is so much reduced, implying that the most of incident energy is transmitted into the bulk. For *p*-polarized wave, if incident angle is close to Brewster's angle, this reduction should be possible. In fact, $\hat{\imath}'(x_1)$ of (4, 1, 1) is the largest among those of four profiles. This is the reason for the reduction. If we further decrease the width comparable to wavelength, we enter diffractive regime. Then we should expect diffusive scattering as in Fig. 13. Even more decrement of the well width should recover the Fresnel result. Figure 14 and 15 show DRC's when $\grave{e}_i = 10^\circ$, 40° and 65° of (4, 1, 1) and (4, 1, 0.02) cases respectively. Both profiles seem to scatter incident beam in most diffusive way. These computed DRC's include all the effects of multiple scattering, surface shadowing and diffraction. It looks like that more multiple scatterings are involved in (4, 1, 1) compared to (4, 1, 0.02) .

IV. CONCLUSION

We have computed DRC's for several well profiles and examined how DRC varies as we change well depth, slope or width. DRC's were computed based on the second Green's theorem which should be exact even in diffractive regime. The

purpose of this computation was to determine the class of surface profiles which causes most diffusive scattering.

At normal incidence, it is hard to get diffusive scattering unless the well width is comparable to beam waist radius W_o. But at oblique angles, narrow and deep well gives rise to multiple scattering as well as diffraction so that we can have simple but somewhat reasonably efficient diffuser. In this paper, we always set W_o to be less than or equal to the well width. Otherwise the specular reflection will dominate compared to other effects. Therefore to have maximal diffusiveness, the waist radius of Gaussian beam and its wavelength should be comparable to the well width and that well depth has to be larger than a wavelength.

The class of surface profiles is rather limited here. We may use different well shapes. For those new class of profiles, we will probably have much different structures of DRC's. But the arguments would still be the same as stated in Section III. It will also be worth to compute DRC using *p*-polarized beams. We hope to continue this work until we get some practical value out of it.

ACKNOWLEDGMENTS

This work is supported by the Electronics and Telecommunications Research Institute, Korea. We are grateful to department manager D. H. Kim for his support on this research.

REFERENCES

[1] E. R. Méndez, "Enhanced Backscattering of Light from a Random Grating," *Annals of Phys.*, 203, 1990, pp. 255–307.

[2] K. A. O'Donnell and E. R. Méndez, "Experimental Study of Scattering from Characterized Random Surfaces," *J. Opt. Sco. Am. A*, Vol. 4, No. 7, 1987, pp. 1194–1205.

[3] P. Beckmann and A. Spizzichino, *The Scattering of Electromagnetic Waves from Rough Surfaces*, Pergamon, New York, 1993.

[4] A. A. Maradudic and E. R. Méndez, "Enhanced Backscattering of Light from Deterministic Quasi-periodic Surfaces," *Opt. Lett.*, Vol. 17, No. 24, 1992, pp. 1752–1754.

[5] Jun Q. Lu and Zu-Han Gu, "Enhanced Backscattering from One-dimensional Deterministic Surfaces," *J. Opt. Soc. Am. A*, Vol. 13, No. 9, 1996, pp. 1877–1883.

[6] J. T. Lee and W. L. Saich, "Towards the Calculation of Crystallinity Effects on the Surface Optical Response in Metals," *Phys. Rev. B*, 43, 1991, pp. 4629–4635.

[7] B. E. A. Saleh and M. C. Teich, *Fundamentals of Photonics*, John Wiley & Sons, Inc., New York, 1991.

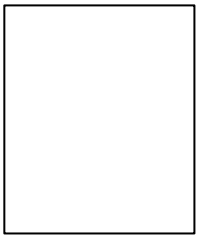

Jong Tai Lee received the B.S. degree in physics education from Seoul National University, Korea in 1984, the M.S. and Ph.D. degrees in physics in 1989 and 1991, respectively, both from Indiana University, USA. Since he joined ETRI in 1992, he has been engaged in the research and development of ATM call control and information security. His current research interests are quantum cryptography and internet security.